Earth and Planetary Science Letters 299 (2010) 118–125

Contents lists available at ScienceDirect

Earth and Planetary Science Letters

journal homepage: www.elsevier.com/locate/epsl

Postseismic variations in seismic moment and recurrence interval of repeating earthquakes

Kate Huihusan Chen [a,*], Roland Bürgmann [b], Robert M. Nadeau [b], Ting Chen [c], Nadia Lapusta [d]

[a] Department of Earth Sciences, National Taiwan Normal University, Taipei, Taiwan
[b] Berkeley Seismological Laboratory, University of California, Berkeley, USA
[c] Seismological Laboratory, California Institute of Technology, Pasadena, California, USA
[d] Division of Engineering and Applied Science and Seismological Laboratory, California Institute of Technology, Pasadena, California, USA

ARTICLE INFO

Article history:
Received 29 April 2010
Received in revised form 13 August 2010
Accepted 23 August 2010
Available online 17 September 2010

Editor: R.D. van der Hilst

Keywords:
repeating earthquake sequences
Parkfield earthquake
postseismic process
recurrence acceleration
rate-and-state models

ABSTRACT

In laboratory experiments, longer stationary contact time leads to larger seismic moment during repeated ruptures. However, not all observations in natural fault systems agree with the prediction. We analyze a subset of 34 M−0.4–2.1 repeating earthquake sequences (RES) from 1987 to 2009 at Parkfield to examine the variation of their recurrence properties in space and time. Following a 2004 M6 earthquake, many of the repeating events have greatly reduced recurrence intervals (*Tr*) that systematically increase with time. In addition to this change in timing, we also find systematic changes in seismic moment (*Mo*), where most sequences experienced an immediate increase in *Mo* and subsequent decay as *Tr* approached pre-quake durations. The RES at shallower depth tend to have a larger range in both *Tr* and *Mo*, whereas deeper RES show smaller variation. The shallowest RES with the greatest magnitude (M1.8–2.1) among the events we studied reveal a large variation in *Tr* but small variation in *Mo*. These observations are qualitatively consistent with earthquake simulations in 3D continuum fault models with rate- and state-dependent friction. In the models, RES are produced on velocity-weakening patches surrounded by velocity-strengthening fault areas. The models show that the degree of postseismic variation in *Mo* and *Tr* is a function of radius (r) and nucleation zone size (h^*) of the velocity-weakening patch. A ratio of $r/h^* \sim 1$ produces negative *Mo*–*Tr* slopes, whereas larger ratios of r/h^* yield weak positive slopes. Given the same nucleation size h^* (i.e., the same frictional properties and effective normal stress), smaller radii and hence smaller seismic moments result in negative *Mo*–*Tr* slopes, whereas larger radii and hence larger moments lead to weak positive *Mo*–*Tr* slopes, which are consistent with observations. Conversely, with only a small percentage of its slip accumulated seismically, a small asperity appears to grow in *Mo* under high loading rate, which is contrary to the view that *Mo* should decrease due to a reduced strength recovery time.

1. Introduction

What governs the variability of earthquake recurrences is of fundamental importance to understanding the earthquake cycle and has important implications for earthquake hazard estimates. Fault interaction, in the form of advances or delays in earthquake recurrence from changes in the stress field by nearby earthquakes and their postseismic deformation transients is believed to play a first-order role (Freed, 2005; Harris, 1998). In some natural fault systems, multiple postseismic repeats of small earthquakes are commonly found after a large event, including the 1984 M6.2 Morgan Hill earthquake (Vidale et al., 1994; Marone et al., 1995; Schaff and Beroza, 2004; Peng et al., 2005; Templeton et al., 2009), 1989 M6.9 Loma Prieta event (Schaff et al., 1998; Schaff and Beroza, 2004), several subduction zone earthquakes in Japan (e.g., Uchida et al., 2004), and the 2004 M6.0 Parkfield earthquake (Taira et al., 2009, Lengline and Marsan, 2009). Pre- and postseismic creep is also found in the subduction zone associated with major earthquakes as derived from RES (Uchida et al., 2004 2006). Along all these fault zones RES and evidence for aseismic slip were observed prior to the mainshocks, suggesting that creep occurs interseismically, as well. Detailed documentation of variation of recurrence interval and seismic moment has been lacking, due to limited historical or paleoseismic data for recurring large repeating earthquakes. Here we use the large number, precisely known relative locations and frequent repeats of small repeating earthquakes at Parkfield, California, to evaluate the effect of transient increase in loading on the timing and moment variations of observed event sequences.

A repeating earthquake sequence (RES) is a group of events that ruptures the same patch of fault repeatedly with nearly identical waveforms, locations, and magnitudes. The recurrence properties of

Abbreviations: RES, repeating earthquake sequences; *Tr*, recurrence time; *Mo*, seismic moment; HRSN, High Resolution Seismic Network; NCSN, Northern California Seismic Network.

* Corresponding author.
E-mail address: katepili@gmail.com (K.H. Chen).

0012-821X/$ – see front matter © 2010 Elsevier B.V. All rights reserved.
doi:10.1016/j.epsl.2010.08.027

RES are suggestive of a renewal process taking place on the repeatedly rupturing fault patches and thus provide crucial information about the nature of the earthquake cycle and the physics of earthquake rupture. After a nearby large earthquake, the observed recurrence intervals (*Tr*) of small repeating earthquakes are dramatically shortened and follow an Omori's law distribution in time as *Tr* recovers, representing accelerated fault creep along some faults surrounding the rupture (Vidale et al., 1994; Marone et al., 1995; Marone, 1998b; Schaff et al., 1998; Peng et al., 2005; Taira et al., 2009). In addition, macroscopic source properties such as earthquake source dimension, rupture velocity, and seismic moment have been found to vary systematically for some postseismic RES (Peng et al., 2005; Taira et al., 2009).

Laboratory experiments imply that fault strength recovery with the time of stationary contact produces a 3–8% increase in static friction for a tenfold increase in recurrence time (Dieterich, 1972; Beeler et al., 1994; Marone, 1998a). If one assumes that the entire fault reaches static friction before failure and that the fault stress after failure is the same, then laboratory inferences of higher static friction predict larger stress drops and hence larger seismic moment for longer stationary contact. Such behavior has indeed been observed. Vidale et al. (1994) studied a RES with 18 events on the Calaveras fault and found that after the 1984 M6 Morgan Hill event, the repeating events with the longest recurrence time (*Tr*) tend to have ~15% larger seismic moment (*Mo*) and possibly ~5% larger patch radius than those with the shortest intervals. Likewise for the 160 RES in the Parkfield, CA area, Nadeau and McEvilly (1999) reported an 18% increase in *Mo* for a 10-fold increase in the preceding *Tr* during a transient slip episode lasting several years. Taira et al. (2009) found that half of a population of 17 RES at Parkfield exhibited similar systematic temporal variation in *Mo* and *Tr* after the Pakfeild event. Given that the stress drop and *Tr* are controlled by the failure of the fault, they suggest that such a correlation may reflect temporal changes of fault strength. In addition to changes associated with the local 2004 M6 Parkfield event, the systematic reduction in *Mo* and *Tr* of Parkfield repeaters also occurred following the regional 1992 M7.3 Landers earthquake and distant 2004 M9.0 Sumatra–Andaman, which Taira et al. (2009) attribute to fault weakening from teleseismic surface waves of both earthquakes.

However, not all observations support the universal increase in seismic moment with increasing recurrence time. Peng et al. (2005) found a depth-dependent *Mo* (calculated from Northern California Seismic Network (NCSN) catalog magnitude estimates) vs. *Tr* trend from a catalog of 194 updated RES in the Calaveras fault study area. In particular, their results showed a negative *Mo* vs. *Tr* trend for the deeper RES, which they hypothesized to be a result of transient embrittlement due to higher strain rates. High strain rates right after the mainshock may cause transient embrittlement in areas directly adjacent to the mainshock, resulting in an increase in *Mo* for the deep repeating clusters in the early postseismic period. As the strain rate decreases with time, these areas would return to a neutrally-stable frictional behavior with concomitant reduction in stress drop.

Here we present detailed observations of the *Tr* and *Mo* variations of post-2004 RES at Parkfield and compare them with the behavior of RES in rate-and-state fault models (Chen and Lapusta, 2009). The observations of Parkfield RES show that *Mo* can exhibit both decreasing and increasing trends with increasing *Tr*, with the negative slopes of the *Mo*–*Tr* relation being more common. Our rate-and-state models produce qualitatively similar behavior. In the models, the behavior of RES, and in particular the *Mo*–*Tr* relation, is not controlled by the increase of static friction in stationary contact. Rather, it is controlled by the patch size and the nucleation size corresponding to patch friction properties, and the associated complex interactions of seismic and aseismic slip.

2. Repeating earthquakes at Parkfield

In Parkfield, the borehole High Resolution Seismic Network (HRSN) has allowed for the identification of a large number of repeating earthquakes down to magnitude −0.4 (Nadeau et al., 1995; Nadeau and McEvilly, 1997, 1999, 2004; Nadeau and Johnson, 1998). Recording of the HRSN deep borehole sensors began in early 1987, but the original data acquisition system failed in 1998. In August 2001, the HRSN network was upgraded and three new borehole stations were installed to improve resolution of the structure, kinematics and monitoring capabilities in the SAFOD drill-path and target zone (Nadeau et al., 2004). Because smaller RES are more numerous and repeat more frequently, the HRSN catalog significantly increases the amount of data available for analysis and provides a better opportunity to examine recurrence properties. During the period 1987–1998, 187 repeating sequences were identified with the total event number of 1117 (Nadeau and McEvilly, 1999; Nadeau and Johnson, 1998) (blue circles in Fig. 1). We consider a subset of 34 updated HRSN RES (red triangles in Fig. 1) for which the observation period was extended from August 2001 to November 2009. They are composed of 837 repeating events (spanning 770 recurrence intervals outside of the 1998–2001 acquisition gap) of which 527 events occurred after the 2004 Parkfield earthquake. These updated sequences provide the opportunity to carefully examine the postseismic process following the 2004 Parkfield earthquake. Identification of the RES events for the extended period was performed by scanning continuous data using a cross-correlation pattern matching approach. A single reference event from each RES was taken as the pattern for scanning for the corresponding RES events. This computationally intensive approach helped optimize completeness of identification. Due to the large computational effort required for the scanning, only a subset of 34 RES was used. Selection of these sequences was largely arbitrary with the only requirement that the RES provide coverage of the fault zone in depth and along strike.

2.1. Recurrence acceleration following the 2004 Parkfield earthquake

Following the 29 September 2004, M6.0 Parkfield earthquake, a strongly accelerated rate of postseismic repeats is observed for 22 of the 34 event sequences. The rapid event recurrences reflect increased loading of the RES asperities by co-seismic stress changes and accelerated fault creep surrounding the 2004 rupture (Johanson et al., 2006; Johnson et al., 2006; Murray and Langbein, 2006). Fig. 2 shows the temporal evolution of recurrence intervals and seismic moment for two example groups (group 2 and SAFOD). The time series of *Tr* and *Mo* for all the RES considered in this study are shown in Figs. S1–S7, where five of the 34 updated RES have not recurred since 2004 (h19, h5, h1 in group 5 and h25, h10 in group 6), suggesting that the Parkfield rupture somehow shut off these larger magnitude RES near the NW end of the rupture front, at least for the time being. Similar observations were also reported by Lengline and Marsan (2009), who examine the recurrence behavior of larger magnitude RES using NCSN data. Of the 26 RES that have post-Parkfield events with a pattern of recurrence acceleration, eight (h9, h13, h14, h15, h18, h26, h33, and h34) have recovered to $\geq$70% of the background *Tr* level (i.e., average *Tr* for the pre-Parkfield events), by 2009. We note that recurrence intervals did vary during the preseismic period reflecting in particular an episode of accelerated fault creep in the early 1990s (e.g., Langbein et al., 1999; Nadeau and McEvilly, 1999; Gao et al., 2000; Murray and Segall, 2005) and the response of RES to five M4–5 earthquakes along the Parkfield fault segment during this time (Chen et al., 2010).

2.2. Seismic moment variation

Rather than relying on the relatively imprecise NCSN catalog coda duration magnitudes, more precise seismic moments are determined by the following steps: (1) aligning P and S arrivals through cross-correlation of repeating events in a sequence, (2) calculating spectra for 0.5 (P) and 1.0 (S) second time windows beginning at the phase arrivals for all operational stations (using vertical component for P and

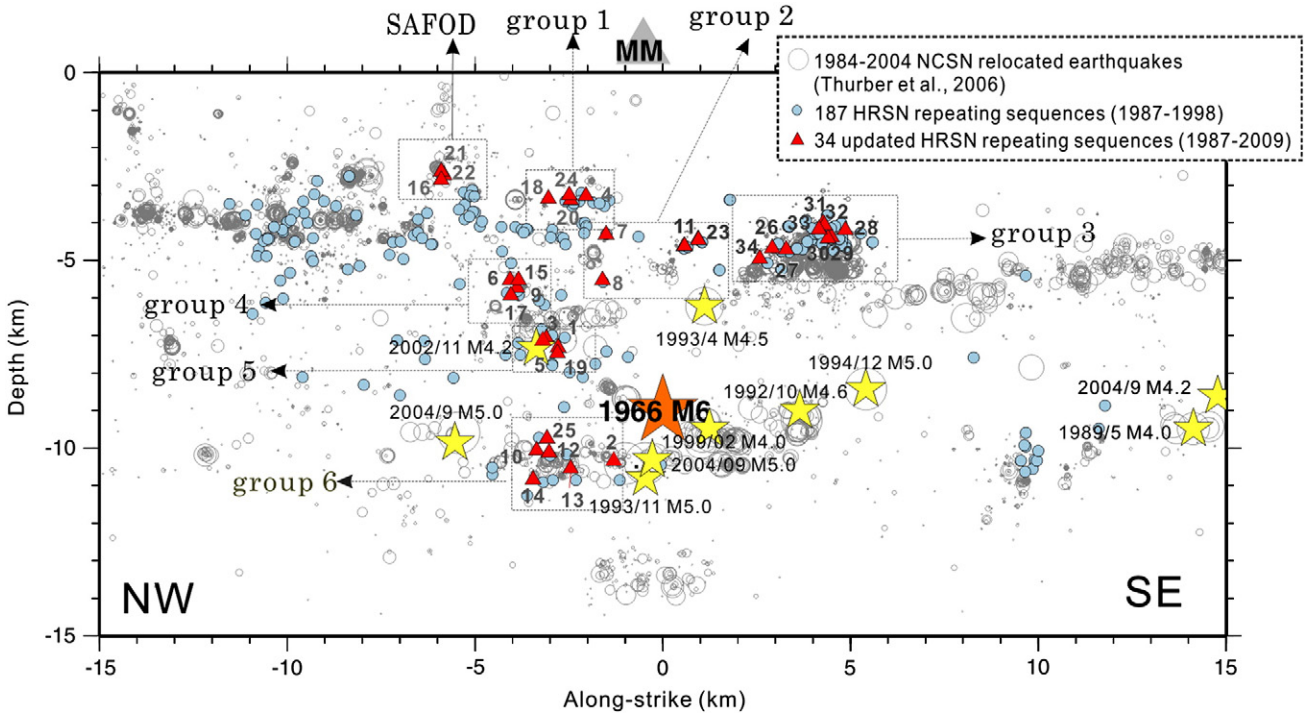

Fig. 1. Along-fault depth section showing the distribution of the 187 HRSN (1987–1998, blue dots) and the 34 updated HRSN repeating earthquake sequences used in this study (1987–2009, red triangles). The 34 updated sequences are spatially clustered into seven groups (SAFOD and groups 1 to 6). Background seismicity (Thurber et al., 2006) is denoted by open circles whose sizes are scaled by magnitude. For reference, the 1966 M6 hypocenter is indicated by an orange star. M4–5 earthquakes that occurred in the 1984–2005 period are denoted by yellow stars. 6).

horizontal components for S when available), (3) calculating low frequency (2 to 22 Hz) spectral ratios for all the selected channels and for all members of the sequence with a reference event (to obtain a consistent network-averaged spectral ratio for each event), and (4) combining these spectral ratio with the average moment tensor solutions for each event (when available) to determine refined absolute seismic moment estimates for each member of each RES. This results in seismic moments with the precision of relative determinations, with more consistent absolute estimates and with estimates of the moments' uncertainties (Nadeau and Johnson, 1998). The precision of the relative moment estimates is ±5% (2 sigma, 95% confidence).

Unlike the sharp decrease and subsequent increase of *Tr* exhibited by most RES following the Parkfield event, changes in *Mo* reveal a larger degree of variability. Fig. 2b shows the temporal evolution of seismic moment for group 2 and SAFOD, with the behavior of all RES given in Figs. S1–S7. Most RES exhibit a notable sudden increase and subsequent decrease of seismic moment shortly after the M 6 event (e.g., Fig. 2b). However, some RES show smaller variability in moment (e.g., Fig. 2d). Overall, the seismic moment of the post-Parkfield events in groups 1 to 4 increases by a factor of 1 to 4.2, with an average of 1.8 and a standard deviation of 0.15 to 0.49. In the shallowest SAFOD group with the largest magnitude events (M1.8–2.1) among the 34 RES, however, the seismic moment changes by a factor of 0.8 to 1.4 (averaging 1.0) and a smaller standard deviation of 0.1 to 0.3. Even though we find a strong reduction in *Tr* for these larger RES, there was an insignificant change in *Mo*.

2.3. Mo–Tr relation

To further explore the variability in seismic moment *Mo* and recurrence interval *Tr*, and to investigate their potential relation, we plot *Mo* vs. *Tr* (Fig. 3, Figs. S1–S7), with *Mo* normalized by the average *Mo* (*Mave*) of the whole sequence. Fig. 3 illustrates the behavior for several groups of shallow RES with postseismic repeats. Repeating event recurrences in each sequence are divided into two periods: pre- and post-Parkfield earthquakes. Pre-Parkfield events (blue dots in Fig. 3) have the longest *Tr* and are confined to a limited range of *Tr* and *Mo*, whereas the immediate postseismic events generally have the shortest *Tr*, as expected. The early postseismic recurrence intervals have a relatively large span (green dots in Fig. 3). The postseismic recurrence intervals increase with time, with some scatter, and gradually approach the preseismic level. Most of the postseismic events in the shallow sequences have larger moments than the preseismic occurrences except for h20, the sequence with the smallest magnitude. About 60% of the post-Parkfield events fail to fully return back to background *Mo* levels (±30% of average pre-Parkfield *Mo*), by November 2009.

To quantify the relation between *Mo* and *Tr*, we fit the postseismic data by $Mo/Mave \sim q \log Tr$ using the least squares method, for the 26 Parkfield RES with more than four postseismic events (following Peng et al., 2005). The fits are shown by dashed lines in Fig. 3 and Figs. S1–S7. Positive/negative slopes *q* of the *Mo*–*Tr* relation correspond to increase/decrease in moment with increasing recurrence time. We find that the negative slope is preferred by the Parkfield RES, with 19 out of 26 RES resulting in the negative slope (Figs. 3 and 4a). Magnitude ranges for the postseismic RES characterized by negative and positive *Mo*–*Tr* slopes are M−0.36–1.82 and M0.64–2.12, respectively. The values of slope *q* show increase with the seismic moment (Fig. 4), with a lot of scatter.

The shallow RES have a larger range in both *Tr* and *Mo*, whereas deeper RES seem to have fewer repeats and show smaller variation in *Tr* and *Mo* (Figs. S6 and S7). The shallowest RES group of SAFOD target events with the greatest magnitudes (M1.8–2.1), however, experience large changes in recurrence interval but only small variations in seismic moment.

3. Rate-and-state models of RES and comparison with observations

To understand factors that control the response of repeating earthquakes to postseismic effects of a large nearby event, we use a 3D fault model based on laboratory-derived rate-and-state friction laws

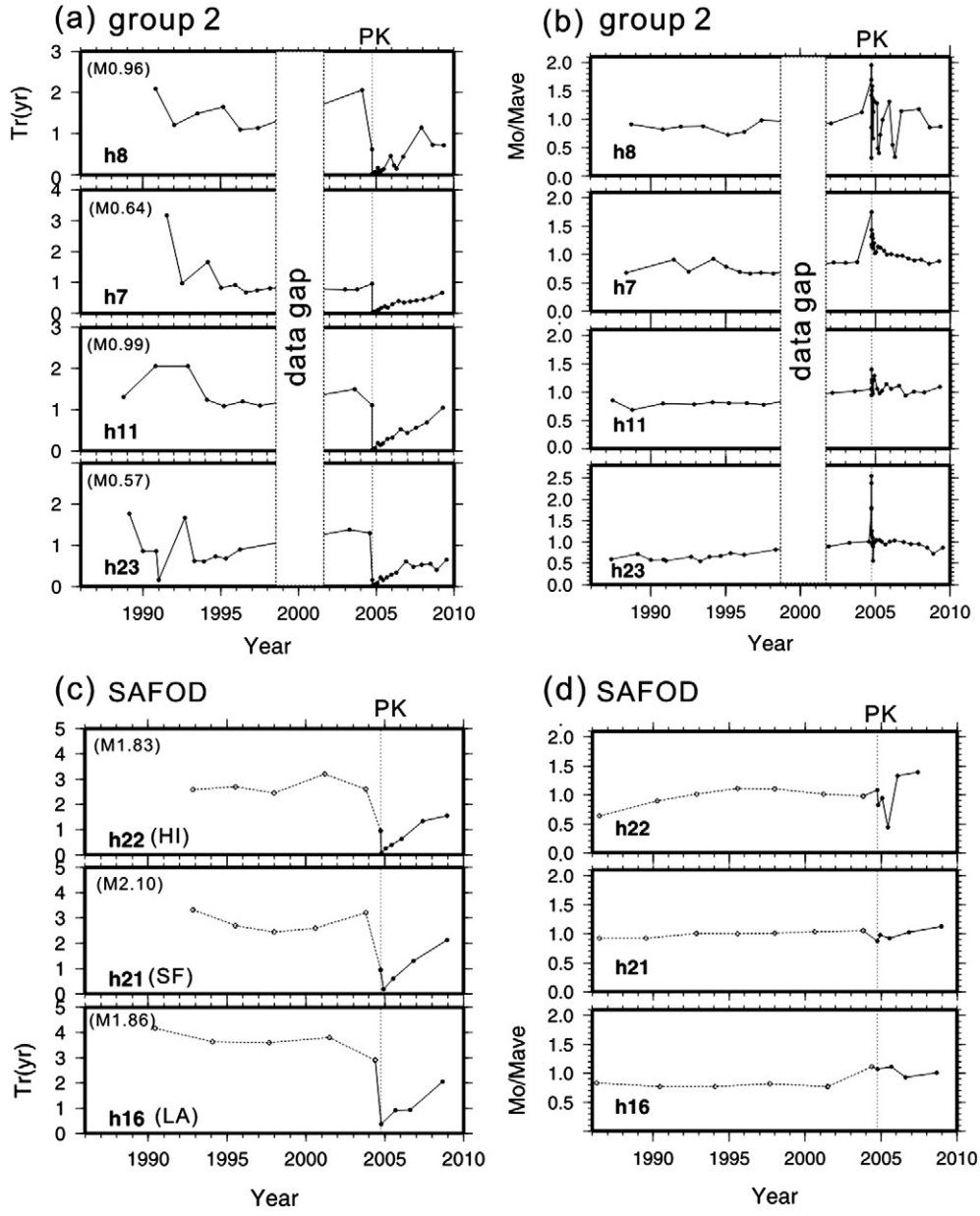

Fig. 2. (a) Recurrence interval as a function of time and (b) relative moment variation (ratio of *Mo* and average *Mo* of the sequence) as a function of time for group 2 repeating sequences. (c) Recurrence interval as a function of time and (d) relative moment variation as a function of time for SAFOD repeating sequences. Vertical dashed line and PK represent the time of the 2004 M6 Parkfield event. The 1998–2001 acquisition gap for the HRSN data is denoted by the white rectangular area in (a) and (b). For SAFOD target events, their recurrence and seismic moment data before August 2001 are from Northern California Seismic Network, as denoted by dashed line in (c) and (d).

with the aging form of state variable evolution (described in detail in Chen and Lapusta, 2009). The model considers a vertical strike–slip fault embedded in an elastic medium. A circular patch with steady-state velocity-weakening properties is surrounded by velocity-strengthening fault areas, with steady sliding at slip velocity VL imposed outside the fault segment (Fig. 5a). The model behavior is simulated using a computation approach that allows to fully resolve both aseismic slip and inertial effects during seismic events (Lapusta and Liu, 2009), enabling realistic representation of seismic events and their interaction with aseismic slip. As shown by Chen and Lapusta (2009), slip partitioning into seismic and aseismic parts can explain the observed scaling for Parkfield repeaters (Nadeau and Johnson, 1998; Johnson, 2010) Modeling the behavior of repeating earthquakes due to static stress perturbations has been shown previously to lead to complex behavior, such as delay of seismic events after favorable stress perturbations due to additional aseismic slip and associated seismic quiescence (Kaneko and Lapusta, 2008).

To study the effect of the Parkfield earthquake, we simulate the consequences of a sudden shear stress increase in the vicinity of an RES by using the following loading velocity history in our simulations:

$$V_L(t) = 23\text{mm/yr}, \quad t<t_p;$$
$$V_L(t) = 23\frac{100\exp[(t-t_p)/t_r]}{1+100\{\exp[(t-t_p)/t_r]-1\}} \quad \text{mm/yr}, \quad t\geq t_p; \tag{1}$$

where t_p is the perturbation time chosen to be large enough so that several earthquake cycles are simulated at the background V_L of 23 mm/yr, V_L increases 100 times at $t=t_p$, the subsequent decay in V_L is representative of postseismic slip based on a spring-slider model (Perfettini and Avouac, 2004), and t_r is set to be either 2 (Fig. 5 and Fig. S8) or 10 (Fig. S9) years. Additionally, at $t=t_p$, a shear stress step is applied to the simulated domain, with the magnitude consistent with the 100-fold increase in slip rates for the velocity-strengthening areas.

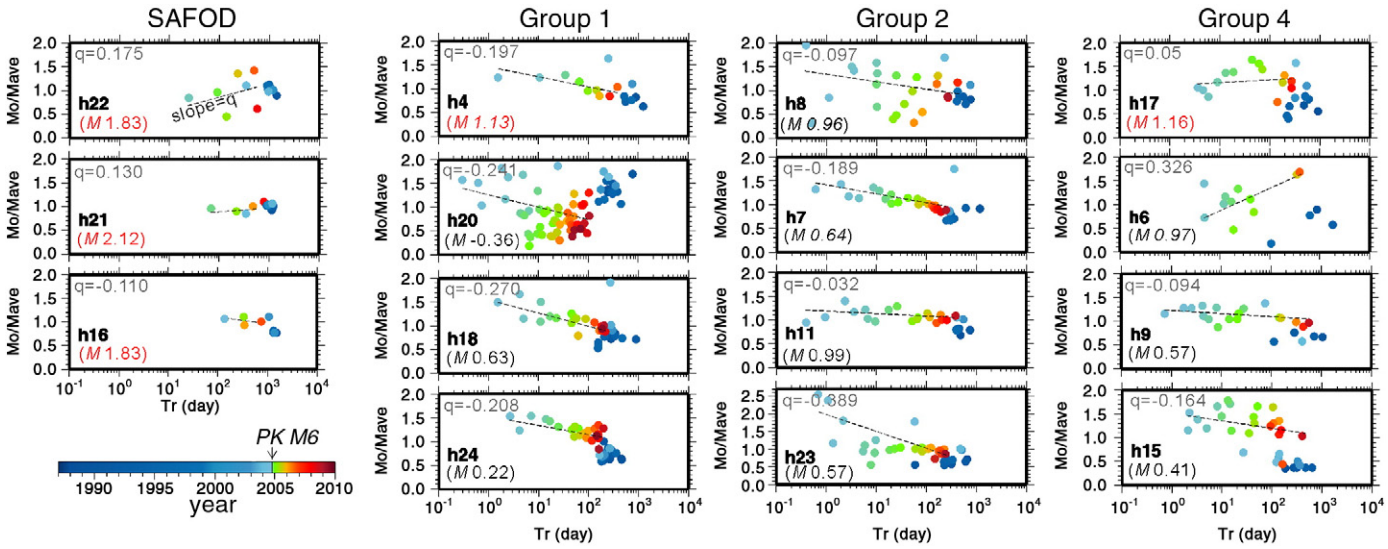

Fig. 3. Relative moment as a function of recurrence interval for SAFOD, groups 1, 2, and 4 RES, color coded by the time of repeating events. Blue and green-to-red dots indicate pre- and post-Parkfield events, respectively. Vertical line on time color scale bar indicates the time of the 2004 M6 Parkfield event. We fit the post-Parkfield data using relative *Mo* (*Mo*/*Mave*) ~ *q* log*Tr* by least squares method, as shown by dashed line (standard error are shown in Figs. S1–S5). *Mave* represents average seismic moment of the sequence.

Our simulations show that the recurrence intervals *Tr* are systematically reduced for larger V_L, as intuitively expected and confirmed by our observations. The simulated moment changes are more interesting, with smaller *Tr* leading to larger moments *Mo* in some cases (Fig. 5b and d) and smaller *Mo* in other cases (Fig. 5c and e), consistent with the richness of our observations (section 2). In the simulations, the sign of the slope for the *Mo*–*Tr* relation is controlled by the ratio r/h^*, where r is the radius of the velocity-weakening patch and h^* is the so-called nucleation size dependent on the friction properties of the patch (Chen and Lapusta, 2009 and references therein):

$$h^* = (\pi^2/4)\cdot \mu b L / \left[\pi(\sigma - p)(b-a)^2\right] \quad (2)$$

In Eq. (2), μ is the shear modulus, $(\sigma - p)$ is the effective normal stress, p is the pore fluid pressure, and a, b and L are friction parameters. Dynamic instability is able to develop (i.e., an earthquake could occur) only if the size of the velocity-weakening patch is comparable to or exceeds the nucleation size h^*, corresponding to ratios r/h^* comparable to or larger than 1 (Chen and Lapusta, 2009 and references therein).

We find that RES with ratios r/h^* comparable to 1 result in negative slope of the *Mo*–*Tr* relation (Fig. 5b and d) while RES with larger r/h^* result in positive slopes (Fig. 5c and e). The difference in the postseismic behavior is related to the difference in the unperturbed behavior for the two cases. For r/h^* comparable to 1, most of the velocity-weakening patch undergoes aseismic slip, and seismic events arise in a small area in the middle of the patch due to stress concentration there (Chen and Lapusta, 2009). Under the faster postseismic loading, the stress concentration in the middle of the patch increases and such events manage to rupture a larger area, resulting in larger seismic moment. In contrast, velocity-weakening patches with larger ratios r/h^* produce events that span the entire patch and the rupture area of the perturbed events stays approximately the same. However, these events tend to have lower stress drop, and hence lower moment, under faster loading. The numerical solutions for the large events are similar to stick–slip simulations with slider blocks (He et al., 2003). The lower stress drops are due to smaller shear stress on the velocity-weakening patch before earthquakes, which occurs due to two reasons. First, in the parts of the velocity-weakening patch which are creeping before an earthquake, the creeping rates are higher for higher loading rates and hence the shear stress is lower (since the patch is rate-weakening). Second, in the parts which are essentially locked, there is less strengthening in stationary contact for shorter recurrence times and hence the shear stress is also lower. In the cases of overall increase of *Mo* with *Tr*, the dependence of *Mo* on *Tr* is weaker and not clearly monotonic (Fig. 5c), which is consistent with observations.

For the same h^*, i.e. for the same friction properties and effective normal stress, larger ratios r/h^* correspond to larger radii r and hence larger unperturbed moments of events, implying that the slope of the *Mo*–*Tr* relation should change from negative to positive for RES with larger magnitudes (Fig. 5b and c). However, different values of r/h^*, and hence both positive and negative slopes of the *Mo*–*Tr* relation, can be achieved for cases with the same unperturbed magnitude by varying the friction properties of the velocity-weakening patches (Fig. 5d and e). Since friction properties of the different Parkfield RES may be different, our simulations suggest that events of comparable *Mo* can have both positive and negative slopes of the *Mo*–*Tr* relation, with a preference for negative slopes for RES of smaller *Mo*.

This is exactly what our Parkfield observations show (Fig. 4a). Parkfield RES with smaller moment ($\log Mo < \sim 17$) exhibit only negative slope, while RES with larger moment exhibit both positive and negative slopes, consistent with the inferences from our model. If our rate-and-state model is representative of these events, the prevalence of the negative slope (in 19 out of 26 RES) implies that most RES considered in this study occur on patches with dimensions just above the nucleation size.

For comparison with observations, Fig. 5 shows only the simulated events with moments that differ less than 0.466 in magnitude from the average unperturbed events. The full response of the model is shown in Fig. S8; it includes events with moments outside of the indicated range. This range is selected based on the observed magnitude variability of the Parkfield RES illustrated in Fig. 6. A total of 837 repeating events shows that the maximum difference in magnitude is 0.466 magnitude units of their sequence average. About 87% of the event magnitudes are within 0.20 magnitude units, and 95% was within 0.29 magnitude units. While there is no explicit magnitude restriction for an event to be selected as a member of a RES, such restriction may be implicit in selecting repeating events based on the similarity of their waveforms.

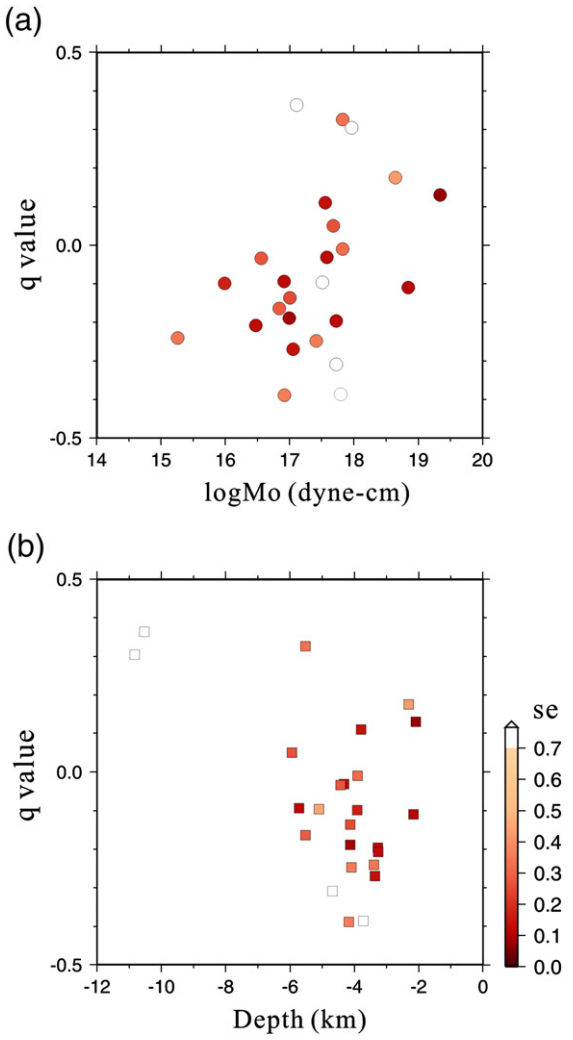

Fig. 4. (a) Average seismic moment of the sequence and (b) q value plotted against depth (i.e., the slope in relative Mo vs. logTr), color coded by least squares method derived standard error (se, standard deviation of the slope).

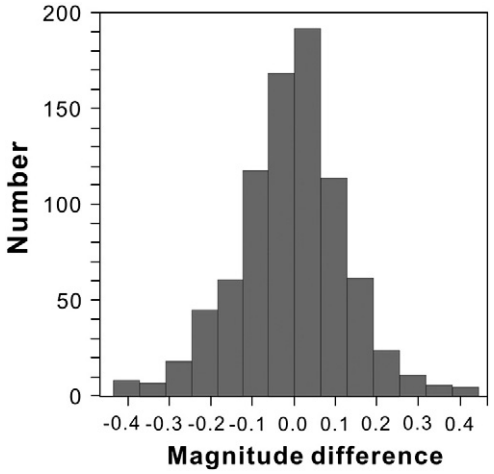

Fig. 6. Histogram of observed differences in repeating events' magnitude from the respective sequence average. Each event's magnitude is subtracted from the average magnitude for the sequence.

4. Discussion

Most post-Parkfield events in the shallower groups 1 to 4 show a systematic trend of decreasing moment with increasing recurrence intervals. At shallow depths (<7 km), the smaller magnitude (M −0.36–1.16) RES reveal a negative slope in *Mo*–*Tr* relation, whereas some of the bigger SAFOD RES (M 1.8–2.1) show a positive slope, although the trend is weak. The larger RES (SAFOD group) show less seismic moment variation after the Parkfield event even through their recurrence intervals decreased just as much as the RES with very small average moments (Fig. 3). Due to the different postseismic recurrence behavior between small and large RES we suggest that the response to a large earthquake and enhanced loading rate from postseismic afterslip is magnitude-dependent. The observed postseismic response can be qualitatively explained by the rate-and-state model.

The post-Parkfield events in the deeper groups 5 and 6 (Figs. S6 and S7) do not exhibit systematic behavior similar to the shallower events. In fact, several RES locations in these groups stopped producing earthquakes after the Parkfield earthquake. In the context of the presented rate-and-state model, such behavior can be explained by the change in the nucleation size h^* due to Parkfield

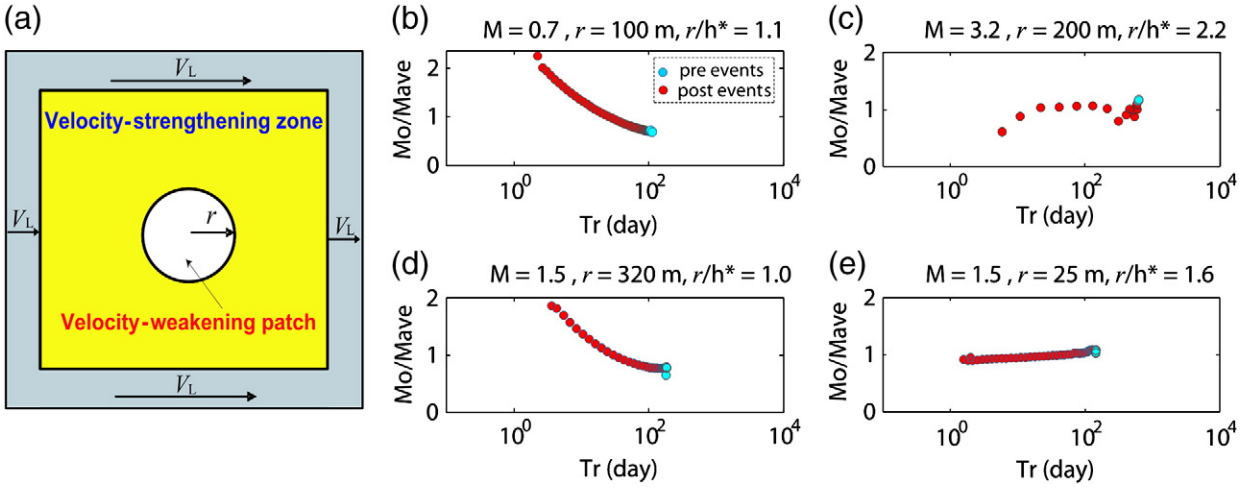

Fig. 5. Simulation results for RES response to postseismic effects of a large nearby event using different model parameters. (a) Fault model for 3-D simulation. A vertical strike–slip fault is embedded into an elastic medium and governed by rate-and-state friction laws as described by Chen and Lapusta (2009). (b–e) Computed relative seismic moment as a function of recurrence interval for varying patch radius r and nucleation size h^* estimated by Eq. (2). Blue and red circles indicate the preseismic and postseismic events, respectively. M is the average magnitude of unperturbed (preseismic) events. Note that only events with moment ranges motivated by observations are shown, as explained in the text. The full model response is given in Fig. S8.

earthquake. If the ratio r/h^* becomes smaller than 1, the patch becomes completely aseismic. The change in h^* could be produced by change in friction parameters due to seismic shaking or by decrease in the effective normal stress due to static stress changes or fluid motion. Hints of some permanent changes of RES properties can be seen in the behavior of group 4 (Fig. 3 and Fig. S5) which shows some post-Parkfield events with recurrence times comparable to pre-Parkfield events but noticeably larger moments.

Based on the rate-and-state model considered in section 3, the observed increase in *Mo* with decreasing *Tr* for most RES studied in this work may be attributed to larger rupture areas for postseismic events. Such larger rupture areas can be achieved because unperturbed events rupture only a part of the velocity-weakening patch. In our model, such situation is created for velocity-weakening patch sizes comparable to the theoretical estimates of nucleation sizes. However, it is possible that similar behavior can result for heterogeneous patches or for patches with a constitutive response that incorporates a stabilizing factor such as dilatancy (e.g., Segall and Rice, 1995).

Note that the rate-and-state friction law used in our model incorporates fault strength recovery in stationary contact observed in the lab (Dieterich, 1972; Beeler et al., 1994; Marone, 1998a). Yet the model does not automatically result in increasing moment with increasing recurrence time. This is because suggestions that fault strength recovery should lead to increase of *Mo* with increasing *Tr* (Vidale et al., 1994; Schaff et al., 1998) are based on simple models that envision earthquake-producing patches reaching static strength over their entire area, as would occur in a single-degree-of-freedom spring-slider approximation. However, the response of the 3D continuum model used in this study is governed by complex multiple-degree-of-freedom interactions, with stress concentrations at the boundaries between creeping and locked regions and combinations of seismic and aseismic slip on the earthquake-producing patches. Hence the presence of fault strength recovery does not lead to easily predictable results, and indeed produces both positive and negative trend of *Mo* with *Tr*, depending on the ratio r/h^*.

Peng et al. (2005) proposed that, *Mo–Tr* relation is depth-dependent, finding a negative *Mo–Tr* trend of the postseismic repeating events at deeper depths along the Calaveras fault (closer to the Morgan Hill mainshock rupture) and a positive trend at shallower depths. We also examine the depth vs. *Mo–Tr* slope relation to see whether the dependency of *Mo–Tr* slope on depth is significant. The selected RES are distributed over a depth range of 2 to 11 km, the corresponding *Mo–Tr* slope values, however, do not reveal a clear trend with the source depth (Fig. 4b). The depth-varying *Mo–Tr* trend found in Peng et al. (2005) is not seen in this study, which indicates the complexity of the postseismic response of RES to the mainshock. One possible explanation is that the deeper RES on the Calaveras fault in Peng et al. (2005) are located right above the mainshock rupture and therefore, may be exposed to a more strongly varying loading rate. The depth-dependent behavior explored in Peng et al. (2005) may thus also be a result of dependency of loading rate. The RES used in this study, on the other hand, are relatively far from the highest co-seismic slip zone (>10 km). Alternatively, the depth-dependent behavior observed by Peng et al. (2005) could be due to systematic variations with depth in ratio r/h^*, present on the Calaveras fault but not in Parkfield. Based on our study, we argue that the dependence of the *Mo–Tr* relation on depth is not obvious. With the increased dynamic range of the upgraded HRSN data and its archival of continuous seismic records, analysis of additional repeating events can be expected to improve our understanding of depth-dependent and/or magnitude-dependent fault processes.

5. Conclusion

The large population of repeating micro-earthquakes at Parkfield provides a unique opportunity to examine, model and test the extent to which fault interaction in the form of static stress changes and transient postseismic fault creep produces changes in frequency and magnitude of the events. Most shallower RES (<7 km) experienced a strong reduction in *Tr* accompanied by an increase in *Mo* immediately following the 2004 Parkfield mainshock, then evolution towards pre-earthquake values in subsequent years. Among the shallow RES, larger events show less variability in seismic moment than small events, even though their transient recurrence acceleration is strong. This magnitude-dependent postseismic behavior can be qualitatively explained by 3-D models using rate-and-state friction laws, in which the repeating events represent rupture of velocity-weakening asperities within an otherwise velocity-strengthening creeping fault zone. In the 3-D simulations, the different degrees to which slip is accommodated aseismically as loading velocity are varied for different asperity radii r and nucleation size h^* leads to different trends between relative moment and recurrence interval. A negative correlation of *Mo–Tr* is predicted if the asperities have $r/h^* \sim 1$ (i.e., smaller asperities for the same h^*), whereas a positive trend is expected for asperities with larger r/h^* (i.e., larger asperity for the same h^*). Asperities comparable in size to h^* tend to accumulate most of their slip aseismically, with earthquakes occupying a small fraction of their area. When experiencing higher loading rates, these small events are found to rupture a larger area of the velocity-weakening asperity, producing the observed behavior of increasing moment with increasing loading rate and decreasing recurrence intervals. For the postseismic period, the good correlation between the observation and model predictions implies that the sudden increase and time-varying loading rate on the velocity-weakening patch play a significant role in a repeater's seismic properties.

The modeling in this study has only explored the behavior of geometrically simple, isolated velocity-weakening patches with homogeneous friction properties and constant effective normal stress. However, the presented study can be expanded to investigate, and compare with observations, the response of seismic moment and recurrence intervals to postseismic loading in the presence of a number of other factors, including spatially heterogeneous friction properties and irregular asperity shapes, interactions between nearby asperities, temporally and spatially nonuniform creeping rates caused by potential heterogeneity of the velocity-strengthening fault areas, variations in effective normal stress due to fluid motion, and time dependence in friction properties caused by the passage of seismic waves. The resulting better understanding of stress-mediated fault interactions and earthquake triggering would enable us to yield improved models of the earthquake cycle and to build more fundamental insight into the underlying physics and mechanics of faults.

Acknowledgements

We are grateful to Nick Beeler, Justin Rubinstein, Doug Dreger, Ruth Harris, and Zhigang Peng for their helpful discussions. We also thank the two reviewers Naoki Uchida and Terry Tullis for their comments to make this paper better. This work was supported by a Southern California Earthquake Center grant (contribution number 1448), the National Science Foundation through grants EAR-0337308, EAR-0537641, EAR-0738342, EAR-0910322, EAR-0544730 and EAR-0510108, Taiwan NSC through grants 98-2116-M-003-002 and 99-2116-M-003-006, and the United States Geological Survey through grant 07HQGR0070. The Parkfield High Resolution Seismic Network is operated by the University of California, Berkeley Seismological Laboratory with financial support from the US Geological Survey (USGS) through National Earthquake Hazards Reduction Program award 07HQAG0014. Seismic data are archived at the Northern California Earthquake Data Center. This is Berkeley Seismological Laboratory contribution 10-11. The numerical simulations for this

research were performed on the Caltech Division of Geological and Planetary Sciences Dell cluster.

Appendix A. Supplementary data

Supplementary data to this article can be found online at doi:10.1016/j.epsl.2010.08.027.

References

Beeler, N.M., Tullis, T.E., Weeks, J.D., 1994. The roles of time and displacement in the evolution effect in rock friction. Geophys. Res. Lett. 21, 1987–1990.

Chen, T., Lapusta, N., 2009. Scaling of small repeating earthquakes explained by interaction of seismic and aseismic slip in a rate and state fault model. J. Geophys. Res. 114 (B01311). doi:10.1029/2008JB005749.

Chen, K.H., Bürgmann, R., Nadeau, R.M., 2010. Triggering effect of M 4–5 earthquakes on the earthquake cycle of repeating events at Parkfield. Bull. Seismol. Soc. Am. 100 (2). doi:10.1785/0120080369.

Dieterich, J.H., 1972. Time-dependent friction in rocks. J. Geophys. Res. 77, 3690–3697.

Freed, A.M., 2005. Earthquake triggering by static, dynamic, and postseismic stress transfer. Annu. Rev. Earth Planet. Sci. 33, 335–368.

Gao, S., Silver, P.G., Linde, A.T., 2000. Analysis of deformation data at Parkfield, California: detection of a long-term strain transient. J. Geophys. Res. 105 (B2), 2955–2967.

Harris, R.A., 1998. Introduction to special section: stress triggers, stress shadows, and implications for seismic hazard. J. Geophys. Res. 103, 24347–24358.

He, C., Wong, T., Beeler, N.M., 2003. Scaling of stress drop with recurrence interval and loading velocity for laboratory-derived fault strength relations. J. Geophys. Res. 108 (B1). doi:10.1029/2002JB001890.

Johanson, I.A., Fielding, E.J., Rolandone, F., Bürgmann, R., 2006. Coseismic and postseismic slip of the 2004 Parkfield earthquake from space-geodetic data. Bull. Seismol. Soc. Am. 96 (4B), S269–S282. doi:10.1785/0120050818.

Johnson, L., 2010. An earthquake model with interacting asperities. Geophys. J. Int. 182, 1339–1373.

Johnson, K.M., Bürgmann, R., Larson, K., 2006. Frictional properties on the San Andreas Fault near Parkfield, California, inferred from models of afterslip following the 2004 earthquake. Bull. Seismol. Soc. Am. 96 (4B), S321–S338. doi:10.1785/0120050808.

Kaneko, Y., Lapusta, N., 2008. Variability of earthquake nucleation in continuum models of rate-and-state faults and implications for aftershock rates. J. Geophys. Res. 113, B12312. doi:10.1029/2007JB005154.

Langbein, J., Gwyther, R., Hart, R., Gladwin, M., 1999. Slip rate increase at Parkfield in 1993 detected by high-precision EDM and borehole tensor strainmeters. Seismol. Res. Lett. 26, 2529–2532.

Lapusta, N., Liu, Y., 2009. Three-dimensional boundary integral modeling of spontaneous earthquake sequences and aseismic slip. J. Geophys. Res. 114, B09303. doi:10.1029/2008JB005934.

Lengline, O., Marsan, D., 2009. Inferring the coseismic and postseismic stress changes caused by the 2004 Mw = 6 Parkfield earthquake from variations of recurrence times of microearthquakes. J. Geophys. Res. 114, B10303. doi:10.1029/2008JB006118.

Marone, C., 1998a. Laboratory-derived friction laws and their application to seismic faulting. Annu. Rev. Earth Planet. Sci. 26, 643–696.

Marone, C., 1998b. The effect of loading rate on static friction and the rate of fault healing during the earthquake cycle. Nature 391, 69–72.

Marone, C., Vidale, J.E., Ellsworth, W.L., 1995. Fault healing inferred from time dependent variations in source properties of repeating earthquakes. Geophys. Res. Lett. 22, 3095–3098.

Murray, J., Langbein, J., 2006. Slip on the San Andreas fault at Parkfield, California over two earthquake cycles and the implications for seismic hazard. Bull. Seismol. Soc. Am. 96 (4B), S283–S303. doi:10.1785/0120050820.

Murray, J., Segall, P., 2005. Spatiotemporal evolution of a transient slip event on the San Andreas fault near Parkfield. J. Geophys. Res. 110, B09407. doi:10.1029/2005JB003651.

Nadeau, R.M., Johnson, L.R., 1998. Seismological studies at Parkfield VI: moment release rates and estimates of source parameters for small repeating earthquake. Bull. Seismol. Soc. Am. 88, 790–814.

Nadeau, R.M., McEvilly, T.V., 1997. Seismological studies at Parkfield V: characteristic Microearthquake Sequences as Fault-zone Drilling Targets. Bull. Seismol. Soc. Am. 87, 1463–1472.

Nadeau, R.M., McEvilly, T.V., 1999. Fault slip rates at depth from recurrence intervals of repeating microearthquakes. Science 285, 718–721.

Nadeau, R.M., McEvilly, T.V., 2004. Periodic pulsing of characteristic microearthquakes on the San Andreas fault. Science 303, 220–222.

Nadeau, R.M., Foxall, W., McEvilly, T.V., 1995. Clustering and periodic recurrence of microearthquakes on the San Andreas Fault at Parkfield, California. Science 267, 503–507.

Nadeau, R.M., Michelini, A., Uhrhammer, R.A., Dolenc, D., McEvilly, T.V., 2004. Detailed kinematics, structure, and recurrence of micro-seismicity in the SAFOD target region. Geophys. Res. Lett. 31 (L12S08). doi:10.1029/2003GL019409.

Peng, Z., Vidale, J.E., Marone, C., Rubin, A., 2005. Systematic variations in recurrence interval and moment of repeating aftershocks. J. Geophys. Res. 32. doi:10.1029/2005GL022626.

Perfettini, H., Avouac, J.P., 2004. Postseismic relaxation driven by brittle creep: a possible mechanism to reconcile geodetic measurements and the decay rate of aftershocks, application to the Chi-Chi earthquake, Taiwan. J. Geophys. Res. 109 (B02304). doi:10.1029/2003jb002488.

Schaff, D.P., Beroza, G.C., 2004. Coseismic and postseismic velocity changes measured by repeating earthquakes. J. Geophys. Res. 109 (B10302). doi:10.1029/2004JB003011.

Schaff, D.P., Beroza, G.C., Shaw, B.E., 1998. Postseismic response of repeating aftershocks. Geophys. Res. Lett. 25 (24), 4549–4552.

Segall, P., Rice, J.R., 1995. Dilatancy, compaction, and slip instability of a fluid infiltrated fault. J. Geophys. Res. 100, 22155–22171.

Taira, T., Silver, P.G., Niu, F., Nadeau, R.M., 2009. Remote triggering of fault-strength changes on the San Andreas fault at Parkfield. Nature 461, 636–639. doi:10.1038/nature08395.

Templeton, D.C., Nadeau, R.M., Bürgmann, R., 2009. Distribution of postseismic slip on the Calaveras fault, California, following the 1984 M6. 2 Morgan Hill earthquake. Earth Planet. Sci. Lett. 277 (1–2), 1–8.

Thurber, C., Zhang, H., Waldhauser, F., Hardebeck, J., Michael, A.J., Eberhart-Phillips, D., 2006. Three-dimensional compressional wavespeed model, Earthquake relocations, and focal mechanisms for the Parkfield. California Bull. Seismol. Soc. Am. 96, S38–S49.

Uchida, N., Hasegawa, A., Matsuzawa, T., Igarashi, T., 2004. Pre- and post-seismic slip on the plate boundary off Sanriku, NE Japan associated with three interplate earthquakes as estimated from small repeating earthquake data. Tectonophysics 385, 1–15.

Uchida, N., Matsuzawa, T., Hirahara, S., Hasegawa, A., 2006. Small repeating earthquakes and interplate creep around the 2005 Miyagi-oki earthquake (M7.2). Earth Planets Space 58, 1577–1580.

Vidale, J.E., Ellsworth, W.L., Cole, A., Marone, C., 1994. Rupture variation with recurrence interval in eighteen cycles of a small earthquake. Nature 368, 624–626.